IEEE Access
Multidisciplinary | Rapid Review | Open Access Journal

Received June 9, 2020, accepted June 15, 2020, date of publication June 18, 2020, date of current version June 30, 2020.

Digital Object Identifier 10.1109/ACCESS.2020.3003319

Quasi-Elliptic Bandpass Frequency Selective Surface Based on Coupled Stubs-Loaded Ring Resonators

RUI-XIANG LIAO[1,2], SAI-WAI WONG[1], (Senior Member, IEEE), YIN LI[1], (Member, IEEE), JING -YU LIN[3], (Student Member, IEEE), BAI-YANG LIU[1], (Member, IEEE), FU-CHANG CHEN[2], (Member, IEEE), AND ZHI QUAN[1], (Senior Member, IEEE)

[1]College of Electronics and Information Engineering, Shenzhen University, Shenzhen 518060, China
[2]School of Electronics and Information Engineering, South China University of Technology, Guangzhou 510640, China
[3]School of Electrical and Data Engineering, University of Technology Sydney, Ultimo, NSW 2007, Australia

Corresponding author: Yin Li (yb57430@connect.umac.mo)

This work was supported in part by the Shenzhen Science and Technology Programs under Grant JCYJ20180305124543176 and Grant JCYJ20190808145411289, in part by the Natural Science Foundation of Guangdong Province under Grant 2018A030313481, in part by the Shenzhen University Research Startup Project of New Staff under Grant 860000002110311, and in part by the Guangdong Basic and Applied Basic Research Foundation under Grant 2019A1515111166.

ABSTRACT In this paper, a novel design of frequency-selective surface (FSS) based on coupled stubs-loaded ring resonators (SLRRs) is proposed. The proposed FSS exhibits quasi-elliptic bandpass filtering characteristic at C-band. And each unit cell of the structure is composed of two SLRRs coupled by a circular aperture. A novel method of transmission line (TL) model is proposed to investigate the operating principle of a single SLRR under normal incidence plane wave. Moreover, the operating mechanism of the proposed FSS is further researched with the aid of the equivalent circuit model (ECM) analysis method. Due to the symmetric and low-profile physical structure, the FSS keeps stable frequency response under oblique incident plane wave for both transverse electric (TE) and transverse magnetic (TM) polarizations. Finally, the designed FSS is fabricated and measured. The measured results agree well with the simulated results. The measured results indicate that the proposed FSS exhibits a dual-polarized and stable bandpass frequency response with two transmission zeros (TZs) at around 5.71 and 6.87 GHz under different incident angles up to 40°.

INDEX TERMS Quasi-elliptic, bandpass, frequency-selective surface (FSS), stubs-loaded ring resonator (SLRR).

I. INTRODUCTION

Frequency-selective surfaces (FSSs) have been intensively researched as spatial filters over the past several decades [1], [2]. Unlike conventional planar microwave filters, the filtering response of FSSs is determined not only by the frequency but also by the incident angle and polarization of the impinging electromagnetic wave. Due to the specific filter properties, FSSs have been applied as various microwave components such as antenna subreflectors [3], [4], antenna radomes [5], [6], absorbers [7], [8] and so on. In many commercial applications, FSSs are usually required to obtain bandpass frequency response. And it makes a lot of sense to design bandpass FSSs with good performance like sharp roll-off, low-profile, and high frequency selectivity.

In recent years, many approaches have been reported to design high perform bandpass FSS. In [9], a bandpass FSS based on antenna-filter-antenna (AFA) module was presented. A third-order bandpass filtering response was achieved by the two back-to-back microstrip patch antennas and the coplanar-waveguide (CPW) resonator in the middle layer. In [10], a quasi-elliptic bandpass FSS is designed based on the composition of metal cylinder pipes and circular patches. A type of low-profile FSS with non-resonant constituting elements was proposed in [11], [12]. The non-resonant elements are composed of capacitive sub-wavelength patches

The associate editor coordinating the review of this manuscript and approving it for publication was Chinmoy Saha.

or inductive wire grids printed on substrates. Parallel *LC* resonators, used to design multi-order bandpass FSS, can be achieved by cascading these non-resonant elements. However, this type of FSS was usually exhibiting a poor frequency selectivity response without finite transmission zeros (TZs). Besides, a bandpass FSS based on coupled circular plates is proposed in [13]. The FSS is achieved by inserting circular dielectric resonators into a metal plate. Due to the signal coupling path, the FSS only exhibits a bandpass frequency response without TZs. Different from traditional FSSs based on two-dimensional (2-D) structure, many three-dimensional (3-D) FSSs have also been studied to realize more attractive filtering characteristics. In [14], [15], several 3-D FSSs based on substrate integrated waveguide (SIW) technology were researched. Cross coupling can be realized by cascading SIW cavities. Thus TZs can be induced to enhance the selectivity. Whereas this kind of FSSs possesses frequency characteristics of narrow band, high selectivity, and a little large insertion loss. A new concept of designing 3-D FSS based on a 2-D periodic array of shielded microstrip lines has been reported in [16], [17]. Propagating modes can be excited by the dispersion diagram of shielded microstrip lines. And filtering performance can be achieved by controlling their cross coupling with air. However, these 3-D FSSs only operate under single polarization are usually difficult to fabricate and assemble.

In this paper, a novel bandpass FSS based on coupled stubs-loaded ring resonators (SLRRs) is investigated and discussed. Although the coupled structure FSS was first proposed in [18], the FSS usually exhibits a bandpass frequency response without any TZs located near the passband due to dominant magnetic coupling and weak electric coupling [19]. While the proposed FSS utilizes back-to-back cascaded SLRRs to enhance electric coupling, which makes it possible to obtain two finite TZs to improve the frequency selectivity. In order to explore the working principle of the FSS, a transmission line (TL) model method is proposed to study the working principle of single SLRR under normal incident plane waves. An equivalent circuit model (ECM) is also established and investigated for a further study of the proposed FSS. Benefit from the low-profile and symmetrical structure, the proposed FSS shows a very stable quasi-elliptic filtering performance under oblique incident wave for both transverse electric (TE) and transverse magnetic (TM) polarizations. Finally, a prototype is fabricated and measured to verify the design.

II. DESIGN AND ANALYSIS OF THE PROPOSED FSS

A. GEOMETRY OF THE PROPOSED FSS

Fig. 1 presents the 3-D geometries of the proposed FSS. The proposed structure is mainly composed of three metal layers, which are stacked together with two thin dielectric-slabs. The top and bottom metal layers are composed of SLRR arrays. The SLRR is an improved ring resonator with eight identical opened stubs periodically loaded, the width of w, and length of h. The angle between every two adjacent opened stubs

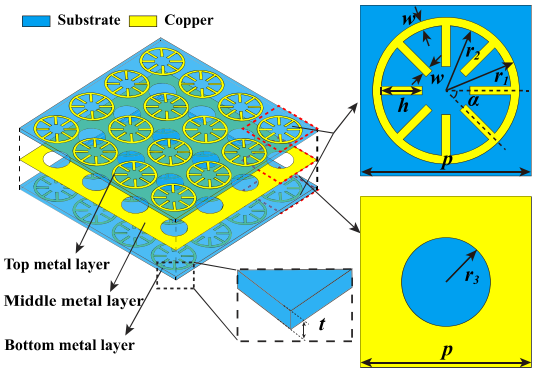

FIGURE 1. 3-D geometries of the proposed FSS.

is α ($\alpha = 45°$), which divides the ring into eight equal parts. The outer and inner radius of the ring are r_1 and r_2, respectively. And it is worth mentioning that the width of the ring strip is equal to the width of the loaded-stubs. The middle metal layer is etched with circular apertures with a radius of r_3 to construct coupling paths between the top and bottom SLRRs. Moreover, the unit cells of the proposed FSS are arranged along the x-direction and y-direction with a period of p. The thickness of the substrate layer is t. The supporting substrate used in this design is Rogers 4003C with relative dielectric constant $\varepsilon_r = 3.38$ and loss tangent of 0.0027.

B. ANALYSIS OF A SINGLE SLRR

SLRR is a deformation product of a conventional ring resonator. And the opened stubs loaded on the ring will significantly affect the resonant frequency of the SLRR. Thus, in this section, a new method based on TL model to extract the resonant frequency of SLRR is proposed. Fig. 2 depicts the schematic of a single SLRR with ground, which is excited by a plane electromagnetic wave. For a more intuitive analysis, the SLRR rotates 22.5° clockwise, which will not influence the resonant frequency due to the symmetry of the structure. Under a y-polarized normally incident wave, the SLRR can be considered as being excited by a two-port feed excitation along y-axis.

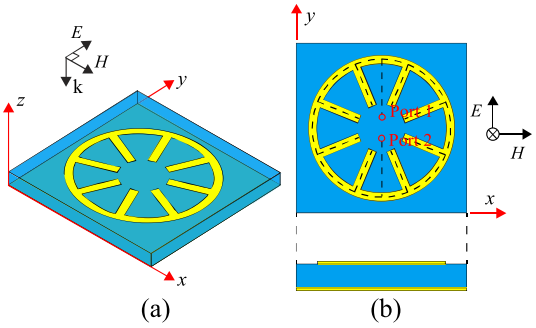

FIGURE 2. Single SLRR with ground. (a) 3D view, (b) Top and side-view.

Based on the discussion above, the performance of a single SLRR can be estimated by a TL model, as depicted

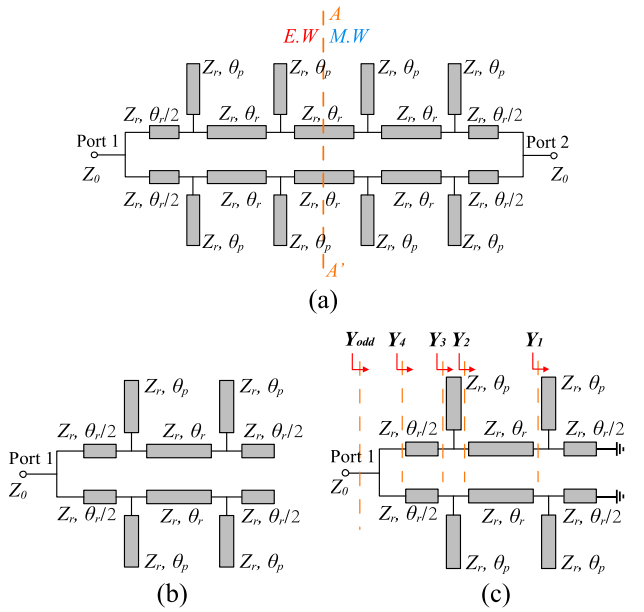

FIGURE 3. Equivalent TL model of the total SLRR. (a) Equivalent TL model of the single SLRR with ground under normal incident wave. (b) Even-mode excitation. (c) Odd-mode excitation.

in Fig. 3(a). As shown herein, $Z_0 = 377\ \Omega$ is the impedance of free space, and Z_r represents the characteristic impedance of the ring with opened stubs. While θ_r is the electrical length of the 1/8 perimeter of ring and θ_p is the electrical length of the loaded opened stubs. The arc attached with the assuming port is divided into two equal parts with the electrical length of θ_r /2. Using the odd- and even-mode analysis method [20], a magnetic wall (an open circuit) and an electric wall (a short circuit) are inserted, subsequently, into the reference plane *AA'* in Fig. 3(a).

Fig. 3(b) and Fig. 3(c) illustrate the even- and odd- mode of TL models, respectively. In the TL model, the two excitation ports, called as port 1 and port 2, are defined to represent the function of the *y*-polarized normally incident wave. Due to the opposite voltage potentials of the two ports, it is obvious that only the odd mode is excited in this model. The odd-mode TL model is investigated to extract the resonant frequency of the SLRR.

Then, the input admittance (Y_1, Y_2, Y_3, Y_4, Y_{odd}) of Fig. 3(c) can be illustrated as follows,

$$Y_1 = jY_r(\tan\theta_p - \cot\frac{\theta_r}{2}) \tag{1}$$

$$Y_2 = Y_r\frac{Y_1 + jY_r\tan\theta_r}{Y_r + jY_1\tan\theta_r} \tag{2}$$

$$Y_3 = Y_2 + jY_r\tan\theta_p \tag{3}$$

$$Y_4 = Y_r\frac{Y_3 + jY_r\tan(\theta_r/2)}{Y_r + jY_3\tan(\theta_r/2)} \tag{4}$$

$$Y_{odd} = 2Y_4 \tag{5}$$

Then, where $Y_r = 1 / Z_r$.

According to (1) - (5), we can obtain and simplify the odd mode input admittance Y_{odd} by software Mathematica,

$$Y_{odd} = -jY_r\csc(\theta_r/2)\left[\cos(2\theta_p - 2\theta_r) + 9\cos(2\theta_p + 2\theta_r) - 2\cos(2\theta_p) + 6\cos(2\theta_r) + 2\right]\Big/\left\{2\left[\cos(\theta_p - \theta_r/2) + 3\cos(\theta_p + \theta_r/2)\right](4\cos\theta_p\cos\theta_r - 2\sin\theta_p\sin\theta_r)\right\} \tag{6}$$

where

$$\theta_r = \frac{\omega_0\sqrt{\varepsilon_{eff}}}{c}\cdot\frac{\pi\,(r_1 + r_2)}{8} \tag{7}$$

$$\theta_p = \frac{\omega_0\sqrt{\varepsilon_{eff}}}{c}\cdot h \tag{8}$$

In which ω_0 represents the angular frequency, and ε_{eff} is the equivalent dielectric constant, which equals to $(\varepsilon_r + 1)/2$ [1]. Under odd mode excitation, the resonance usually occurs at,

$$Im(Y_{odd}) = 0 \tag{9}$$

The resonant frequency of the SLRR can be calculated by solving (9). To further verify the correctness of the TL model, the commercial EM simulator CST Microwave Studio (CST- MWS) is used here to extract the resonant frequency of the SLRR, as full-wave simulated results. The comparison of the resonant frequencies obtained by CST-MWS and the equivalent TL model is illustrated in Fig. 4.

Fig. 4(a) shows the comparison of the results with respect to various h, calculated by full-wave results and the TL model, respectively. The increase of h leads to a larger electrical length θ_p, resulting in a lower resonant frequency. Fig. 4(b) demonstrates the comparison results with respect to various r_1. The electrical length θ_r is mainly determined by r_1. As r_1 increases, the resonant frequency of the SLRR moves toward lower frequency. As a conclusion, the resonant frequencies calculated by the equivalent TL model have good agreements with those obtained by full-wave simulation method. And the calculation error can be controlled within 8%. It is noteworthy that the calculation error is mainly caused by dielectric losses and parasitic effects of the structure in the case of full-wave simulation. Besides, under plane wave excitation, weak couplings between the opened stubs also cause the deviations. In this way, a SLRR resonating at a certain frequency can also be designed with the aid of the equivalent TL model.

C. OPERATING PRINCIPLE OF THE FSS

To research the operating principles of the proposed FSS, a simple ECM is established for normal incidence, as shown in Fig. 5(a). For simplicity, all losses are ignored in the ECM. As ring structure, the SLRRs on the top and bottom layers can be equivalent to the series *LC* circuit (*L* and *C*) [1]. The circular coupling aperture is represented by a parallel *LC* circuit (L_a and C_a) [21]. The air spaces on each side of the FSS can be modeled as a semi-infinite TLs with the characteristic impedance of Z_0. And the two thin dielectric-slabs used for

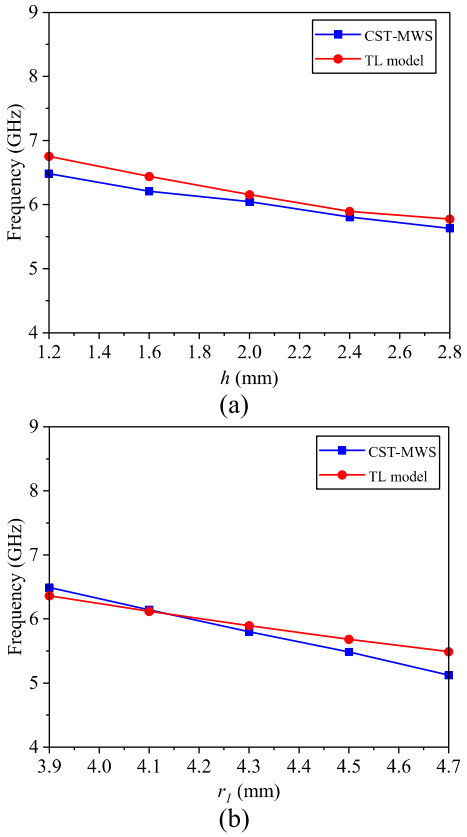

FIGURE 4. Comparison of the resonant frequencies obtained by CST-MWS and equivalent TL model with respect to (a) Length h of the opened stubs ($r_1 = 4.3$ mm, $p = 10$ mm, $w = 0.5$ mm, $\alpha = 45°$, and $t = 0.813$ mm). (b) Outer radius r_1 of the ring ($h = 2.4$ mm, $p = 10$ mm, $w = 0.5$ mm, $\alpha = 45°$, and $t = 0.813$ mm).

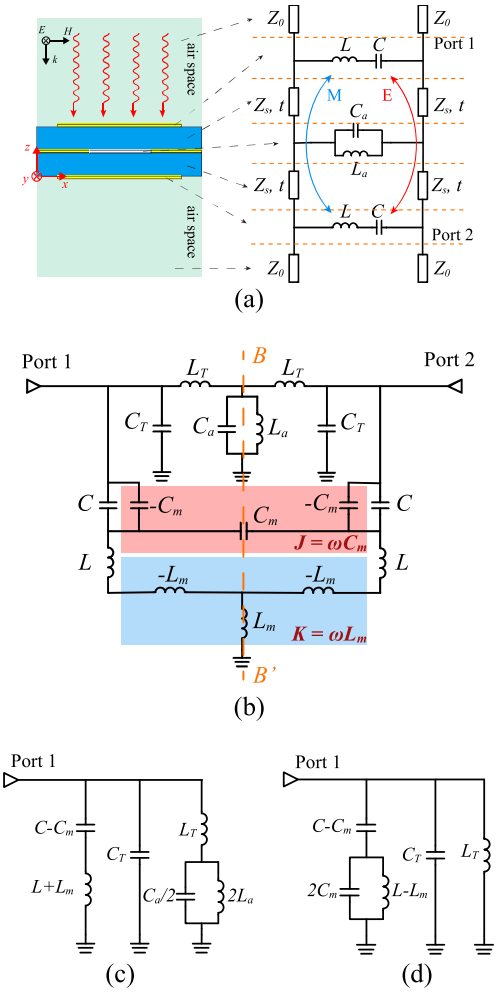

FIGURE 5. ECM of the proposed FSS. (a) ECM of the proposed FSS under normal incidence. (b) Modified ECM of (a). (c) Even-mode model. (d) Odd-mode model.

separating metal layers from one another are represented by TLs with a length of t and a characteristic impedance $Z_s = Z_0/\sqrt{\varepsilon_r}$. The existence of the coupling aperture introduces an electric coupling and a magnetic coupling path, which are denoted by symbols E and M, respectively.

For a more intuitive insight, the ECM in Fig. 5(a) can be converted into the one exhibited in Fig. 5(b), according to some equivalent relations. Actually, the electric coupling between the two SLRRs can be considered as an admittance inverter $J = \omega C_m$. The magnetic coupling can be considered as an impedance inverter $K = \omega L_m$ [22]. Due to the effects of the circular aperture on the middle metal layer, the L and C satisfy the relations, $L = L_0 + L_m$ and $C = C_0 + C_m$. The L_0 and C_0 are the self-inductance and self-capacitance of the resonator without the effects of the coupling aperture [23]. The electrical length of the transmission line is so small ($t < \lambda_0 / 12$, λ_0 is the free space wavelength) that the short transmission lines in Fig. 5(a) are replaced with their ECM composed of a series inductor L_T and a shunt capacitor C_T. Based on the telegrapher's model for TEM transmission line, L_T and C_T can be calculated by following equations:

$$L_T = \mu_0 \mu_r t \tag{10}$$

$$C_T = \varepsilon_0 \varepsilon_r t/2 \tag{11}$$

where μ_0 and ε_0 are the permeability and permittivity of the free space, and μ_r is the relative permeability of the dielectric substrate.

Due to the symmetry of the ECM in Fig. 5(b), it can also be investigated using odd- and even-mode analysis method. Replacing the symmetry plane BB' by a magnetic wall (an open circuit) and an electric wall (a short circuit), respectively. The even-mode circuit model and the odd-mode one can be obtained as shown in Fig.5(c) and (d). And their input admittance can then be expressed as,

$$Y_{even} = \left[\frac{1}{j\omega C_0} + j\omega\left(L + 2L_m\right)\right]^{-1} + j\omega C_T + \left[\frac{2}{j\omega C_a + \frac{1}{j\omega L_a}} + j\omega L_T\right]^{-1} \tag{12}$$

$$Y_{odd} = \left[\frac{1}{2j\omega C_m + \frac{1}{j\omega L_0}} + \frac{1}{j\omega C_0}\right]^{-1} + j\omega C_T + \frac{1}{j\omega L_T} \tag{13}$$

From the mechanism of the resonator resonance, the resonance for both the odd- and even-mode can be calculated by $Y_{even} = 0$ and $Y_{odd} = 0$, respectively. And the frequencies of TZs can be obtained by the equation $Y_{even} = Y_{odd}$ [24].

And then, the scattering parameters can be calculated by following equations [25],

$$S_{11} = \frac{Y_0^2 - Y_{even}Y_{odd}}{(Y_0 + Y_{even})(Y_0 + Y_{odd})} \tag{14}$$

$$S_{21} = \frac{Y_{odd}Y_0 - Y_{even}Y_0}{(Y_0 + Y_{even})(Y_0 + Y_{odd})} \tag{15}$$

where $Y_0 = 1/Z_0$.

If the circuit parameters are known, the scattering parameters of the ECM can be obtained by combining (12) - (15). While the initial circuit parameters can be extracted with the method proposed in [26]. And then, the final circuit parameters can be determined with curve-fitting method. The Optimized parameters are given in Table 1. Fig. 6 shows the comparison of scattering parameters obtained from the CST-MWS and ECM, where good agreement can be observed. And the full-wave simulation results indicate that the proposed FSS can provide a passband with two transmission poles, located at 5.93 GHz and 6.00 GHz. Moreover, it also generates TZs on each side of the passband, which is around 5.71 GHz and 6.87 GHz respectively. It is noteworthy that the discrepancy of the curves obtained from CST-MWS and ECM is mainly due to the fact that the mutual coupling between SLRR and the coupling aperture is ignored in the ECM. Another influencing factor is that the couplings between the loaded-stubs of the SLRR are ignored when establishing the ECM, which cannot be eliminated in EM simulation.

TABLE 1. The optimized parameters of the ECM.

L_0	C_0	L_m	C_m
6.229 nH	0.091 pF	0.006 nH	0.0054 pF
L_a	C_a	L_T	C_T
0.14 nH	0.47 pF	1.02 nH	0.012 pF

In this design, the total coupling k can be extracted by the classical definition as [21], [25],

$$k = \frac{f_{odd}^2 - f_{even}^2}{f_{odd}^2 + f_{even}^2} = \frac{M_C - E_C}{1 - M_C E_C} \tag{16}$$

where E_C is the electric coupling and M_C is the magnetic coupling. It can be observed from (16) that the E_C and M_C tend to cancel with each other, which makes it possible to introduce TZs [19], [21].

The TZ1 locates in lower stopband is generated by canceling effects of the electric and magnetic coupling [19]. It means that the TZ1 can be controlled by adjusting the total coupling. In this design, the loaded open stubs can induce strong electric coupling and weak magnetic coupling. The total coupling can be adjusted by changing the length of the loaded open stubs h. Fig. 7 depicts that the normalized

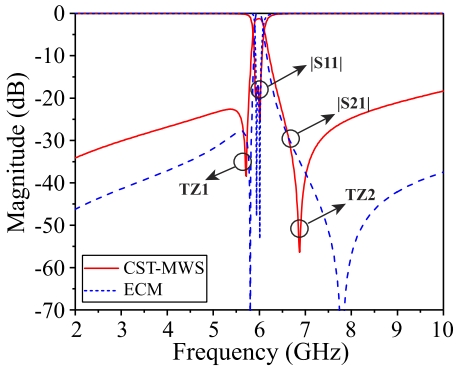

FIGURE 6. S-parameters results of the proposed FSS obtained by the CST-MWS simulation and ECM (Physical dimensions: $r_1 = 4.3$ mm, $r_3 = 2.6$ mm, $p = 10$ mm, $w = 0.5$ mm, $h = 2.4$ mm, $\alpha = 45°$, $\varepsilon_r = 3.88$, and $t = 0.813$ mm).

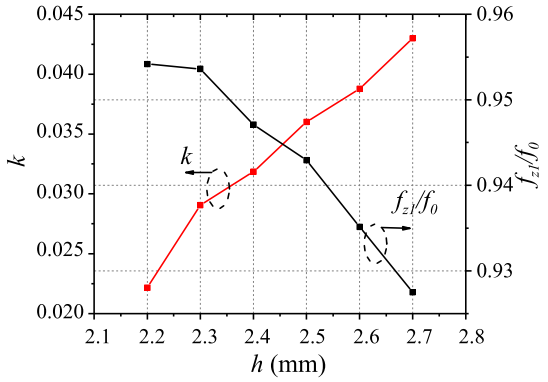

FIGURE 7. k and f_{z1}/f_0 respect to h.

frequency of TZ1 (f_{z1}/f_0) and coupling coefficient k vary significantly by changing the value of h. When h increases, the coupling is enhanced. The TZ1 moves away from passband. While the other finite TZ2 located in upper stopband is mainly caused by the harmonic effects [19], [21].

III. FABRICATION AND MEASUREMENTS

In order to validate the performance of the proposed design, a prototype was manufactured by using the standard printed circuit board (PCB) processing technology. Fig. 8(a) shows the photograph of the fabricated prototype, which is equal to 210 mm ×210 mm in size and contains 433 unit cells. Herein, the prototype was fabricated on two Rogers 4003C substrates (substrate thickness of 0.813 mm and copper thickness of 0.035 mm). There are eight via holes around the peripheries of the fabricated prototype as shown in Fig. 8(a) to fix the two layers by plastic screws. The detailed physical parameters are the same as the ones mentioned in Fig. 6. Then, the fabricated FSS is measured in free space using two horn antennas in a semi-open environment. Fig. 8(b) exhibits the photograph of the FSS measurement setup, which is similar to the one described in [27].

The measured and simulated results under normal incidence are depicted in Fig. 9. A relatively good agreement

TABLE 2. Comparison of performance with the reported FSSs.

Ref.	Unit cell size and thickness	Process difficulty	Installation	Bandwidth(3 dB)	Angular stability	Polarization	TZs near passband
[9]	$0.653\lambda_0 \times 0.653\lambda_0 \times 0.12\lambda_0$	Simple	Easy	8.2%	25°	Single	1
[10]	$0.645\lambda_0 \times 0.645\lambda_0 \times 0.265\lambda_0$	Moderate	Easy	15.2%	20°	Dual	3
[11]	$0.168\lambda_0 \times 0.168\lambda_0 \times 0.04\lambda_0$	Simple	Easy	11.8%	40°	Dual	1
[13]	$0.42\lambda_0 \times 0.42\lambda_0 \times 0.14\lambda_0$	Moderate	Moderate	20%	40°	Dual	0
[17]	$0.094\lambda_0 \times 0.094\lambda_0 \times 0.18\lambda_0$	Complex	Difficult	67%	60°	Dual	1
This work	$\mathbf{0.2\lambda_0 \times 0.2\lambda_0 \times 0.0325\lambda_0}$	**Simple**	**Easy**	**5.1%**	**40°**	**Dual**	**2**

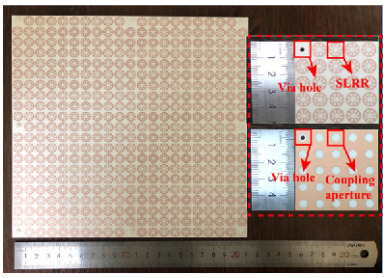

(a)

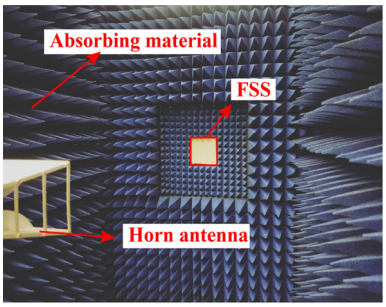

(b)

FIGURE 8. Fabrication and measurement. (a) Fabricated FSS sample including a detail view. (b) Photograph of measurement setup.

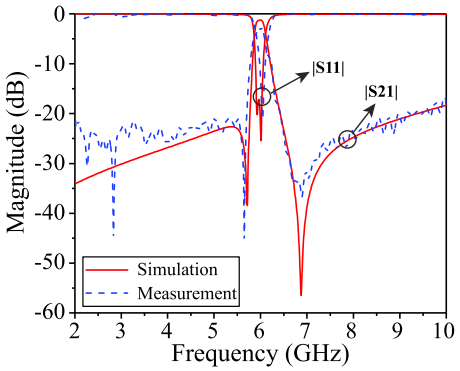

FIGURE 9. Measured and simulated S-parameters results of the proposed FSS under normal incidence.

between measured results and simulated results is observed. The fabricated FSS exhibits a quasi-elliptic bandpass frequency response with a center frequency of 6.02 GHz

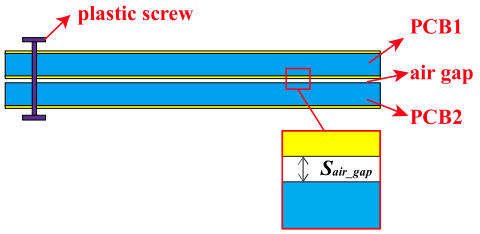

FIGURE 10. The installation diagram of the FSS prototype.

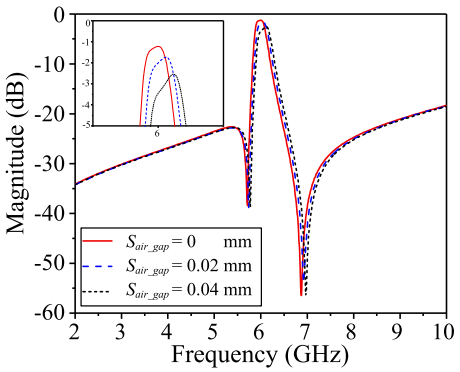

FIGURE 11. Transmission coefficients of the FSS respect to S_{air_gap}.

(5.96 GHz in full-wave simulation). The measured 3-dB bandwidth of passband is 0.31 GHz (0.27 GHz in full-wave simulation), which indicates a relative bandwidth of 5.1%. The measured insertion loss at the center frequency of the passband is 2.5 dB under normal incidence, which is greater than the simulated one of 1.2 dB. The slightly larger measured insertion loss and slightly higher operating frequency are mainly caused by the fabrication tolerance, material parameters difference, and measurement errors. The prototype is fabricated by two layers of PCB. Several plastic screws are used to fix and stack the two boards together. While this method cannot eliminate the ultrathin air space between the two PCBs, as shown in Fig. 10. And the air gap will destroy the insertion loss a lot. Fig. 11 illustrates the transmission coefficients of the FSS respect to different thickness of the air gap, denoted as S_{air_gap}. It can be found that the insertion

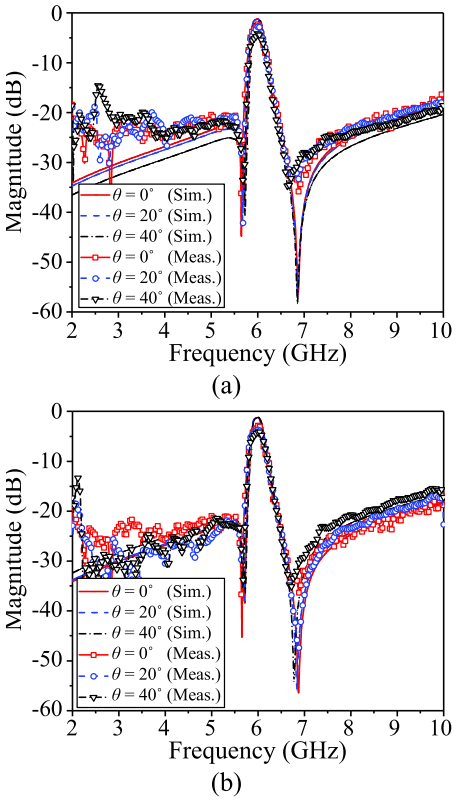

FIGURE 12. Measured and simulated transmission coefficients of the proposed FSS under oblique incidence for. (a) TE polarization. (b) TM polarization.

loss increases with S_{air_gap} raising. When S_{air_gap} equals to 0.02 *mm*, the simulated result of loss increases is close to the measured result. And it hard to realize that S_{air_ga} is smaller than 0.02 *mm* by using the plastic screws. The simulated results also demonstrate the design is feasible.

Moreover, the measured and simulation transmission coefficients of the fabricated FSS for TE and TM polarizations under various incident angles (0°, 20°, and 40°) are exhibited in Fig. 12. The frequency responses of the FSS are stable to varied incident angles and polarizations. When the incidence angle becomes larger, the insertion loss increases, which is mainly determined by the unit size of the FSS comparing to the operating wavelength for a large incident angle. Table 2 shows the performance comparison of the proposed FSS and those reported in other works. It indicates that the proposed structure has the advantages of high selectivity, stable frequency response, and much easy to process.

IV. CONCLUSION

A novel FSS based on SLLRs with a quasi-elliptic bandpass response has been presented in this paper. An equivalent TL model has been established to extract the resonant frequency of the SLRR. Furthermore, an ECM has been investigated using the odd- and even-mode analysis method to further discuss the working mechanism of the proposed FSS. After that, a prototype has been manufactured and measured to verify the design. Both the simulated and measured results have shown that the proposed FSS has a stable frequency response with high selectivity for TE and TM polarization under oblique incidence wave.

REFERENCES

[1] B. A. Munk, *Frequency Selective Surfaces: Theory and Design*. New York, NY, USA: Wiley, 2000.
[2] B. A. Munk, *Finite Antenna Arrays and FSS*. New York, NY, USA: Wiley, 2003.
[3] V. Agrawal and W. Imbriale, "Design of a dichroic cassegrain subreflector," *IEEE Trans. Antennas Propag.*, vol. AP-27, no. 4, pp. 466–473, Jul. 1979.
[4] S. Agahi and R. Mittra, "Design of a cascaded frequency selective surface as a dichroic subreflector," in *Proc. Int. Symp. Antennas Propag. Soc., Merging Technol.*, vol. 1, May 1990, pp. 88–91.
[5] E. Pelton and B. Munk, "A streamlined metallic radome," *IEEE Trans. Antennas Propag.*, vol. AP-22, no. 6, pp. 799–803, Nov. 1974.
[6] H. Chen, X. Hou, and L. Deng, "Design of frequency-selective surfaces radome for a planar slotted waveguide antenna," *IEEE Antennas Wireless Propag. Lett.*, vol. 8, pp. 1231–1233, 2009.
[7] A. K. Rashid, Z. Shen, and S. Aditya, "Wideband microwave absorber based on a two-dimensional periodic array of microstrip lines," *IEEE Trans. Antennas Propag.*, vol. 58, no. 12, pp. 3913–3922, Dec. 2010.
[8] O. Luukkonen, F. Costa, C. R. Simovski, A. Monorchio, and S. A. Tretyakov, "A thin electromagnetic absorber for wide incidence angles and both polarizations," *IEEE Trans. Antennas Propag.*, vol. 57, no. 10, pp. 3119–3125, Oct. 2009.
[9] A. Abbaspour-Tamijani, K. Sarabandi, and G. M. Rebeiz, "Antenna–filter–antenna arrays as a class of bandpass frequency-selective surfaces," *IEEE Trans. Microw. Theory Techn.*, vol. 52, no. 8, pp. 1781–1789, Aug. 2004.
[10] Z. Zhao, A. Zhang, X. Chen, G. Peng, J. Li, H. Shi, and A. A. Kishk, "Bandpass FSS with zeros adjustable quasi-elliptic response," *IEEE Antennas Wireless Propag. Lett.*, vol. 18, no. 6, pp. 1184–1188, Jun. 2019.
[11] N. Behdad, M. Al-Joumayly, and M. Salehi, "A low-profile third-order bandpass frequency selective surface," *IEEE Trans. Antennas Propag.*, vol. 57, no. 2, pp. 460–466, Feb. 2009.
[12] M. Al-Joumayly and N. Behdad, "A new technique for design of low-profile, second-order, bandpass frequency selective surfaces," *IEEE Trans. Antennas Propag.*, vol. 57, no. 2, pp. 452–459, Feb. 2009.
[13] C. Jin, Q. Lv, J. Wang, and Y. Li, "Capped dielectric inserted perforated metallic plate bandpass frequency selective surface," *IEEE Trans. Antennas Propag.*, vol. 65, no. 12, pp. 7129–7136, Dec. 2017.
[14] G. Qing Luo, W. Hong, Z.-C. Hao, B. Liu, W. Dong Li, J. X. Chen, H. X. Zhou, and K. Wu, "Theory and experiment of novel frequency selective surface based on substrate integrated waveguide technology," *IEEE Trans. Antennas Propag.*, vol. 53, no. 12, pp. 4035–4043, Dec. 2005.
[15] G. Q. Luo, W. Hong, Q. H. Lai, K. Wu, and L. L. Sun, "Design and experimental verification of compact frequency-selective surface with quasi-elliptic bandpass response," *IEEE Trans. Microw. Theory Techn.*, vol. 55, no. 12, pp. 2481–2487, Dec. 2007.
[16] A. K. Rashid, Z. Shen, and B. Li, "An elliptical bandpass frequency selective structure based on microstrip lines," *IEEE Trans. Antennas Propag.*, vol. 60, no. 10, pp. 4661–4669, Oct. 2012.
[17] B. Li, X. Huang, L. Zhu, Y. Zhang, Y. Tang, W.-J. Lu, and Y. Bo, "Bandpass frequency selective structure with improved Out-of-Band rejection using stacked single-layer slotlines," *IEEE Trans. Antennas Propag.*, vol. 66, no. 11, pp. 6003–6014, Nov. 2018.
[18] R. Pous and D. M. Pozar, "A frequency-selective surface using aperture-coupled microstrip patches," *IEEE Trans. Antennas Propag.*, vol. 39, no. 12, pp. 1763–1769, Dec. 1991.
[19] K. Ma, J.-G. Ma, K. Seng Yeo, and M. Anh Do, "A compact size coupling controllable filter with separate electric and magnetic coupling paths," *IEEE Trans. Microw. Theory Techn.*, vol. 54, no. 3, pp. 1113–1119, Mar. 2006.
[20] I. C. Hunter, *Theory and Design of Microwave Filters*. London, U.K.: IEE Press, 2001.
[21] D. S. Wang, P. Zhao, and C. H. Chan, "Design and analysis of a high-selectivity frequency-selective surface at 60 GHz," *IEEE Trans. Microw. Theory Techn.*, vol. 64, no. 6, pp. 1694–1703, Jun. 2016.
[22] J.-S. Hong and M. J. Lancaster, "Couplings of microstrip square open-loop resonators for cross-coupled planar microwave filters," *IEEE Trans. Microw. Theory Techn.*, vol. 44, no. 11, pp. 2099–2109, Dec. 1996.

[23] J.-S. Hong and M. J. Lancaster, "Aperture-coupled microstrip open-loop resonators and their applications to the design of novel microstrip bandpass filters," *IEEE Trans. Microw. Theory Techn.*, vol. 47, no. 9, pp. 1848–1855, Sep. 1999.
[24] Y. Wu, K.-S. Chin, W. Che, K.-C. Chang, and W. Feng, "LTCC multi-layered helical filters with a mixed electric and magnetic coupling structure," *IEEE Trans. Compon., Packag., Manuf. Technol.*, vol. 5, no. 8, pp. 1050–1059, Aug. 2015.
[25] J.-S. Hong and M. J. Lancaster, *Microstrip Filters for RF/Microwave Applications*. New York, NY, USA: Wiley, 2001.
[26] F. Costa, A. Monorchio, and G. Manara, "Efficient analysis of frequency-selective surfaces by a simple equivalent-circuit model," *IEEE Antennas Propag. Mag.*, vol. 54, no. 4, pp. 35–48, Aug. 2012.
[27] Q. Lv, C. Jin, B. Zhang, and R. Mittra, "Wide-passband dual-polarized elliptic frequency selective surface," *IEEE Access*, vol. 7, pp. 55833–55840, 2019.

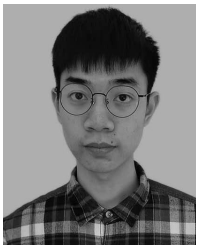

RUI-XIANG LIAO received the B.S. degree in electronic information engineering from Nanchang University, Nanchang, China, in 2017. He is currently pursuing the M.E. degree in electronics and communication engineering with the South China University of Technology, Guangzhou, China. From August 2018 to August 2019, he was a Visiting Student with the College of Electronics and Information Engineering, Shenzhen University, Shenzhen, China. His current research interest includes frequency-selective surfaces.

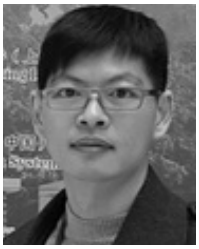

SAI-WAI WONG (Senior Member, IEEE) received the B.S. degree in electronic engineering from The Hong Kong University of Science and Technology, Hong Kong, in 2003, and the M.Sc. and Ph.D. degrees in communication engineering from Nanyang Technological University, Singapore, in 2006 and 2009, respectively.

From July 2003 to July 2005, he was with the Lead Engineering Department of two Hong Kong manufacturing companies, Mainland China. From 2009 to 2010, he was a Research Fellow with the Institute for Infocomm Research, Singapore. Since 2010, he has been an Associate Professor. He has also been a Full Professor with the School of Electronic and Information Engineering, South China University of Technology, Guangzhou, China. In 2016, he was a Visiting Professor with the City University of Hong Kong. In 2017, he was a Visiting Professor with the University of Macau. Since 2017, he has been a Full Professor with the College of Electronic and Information Engineering, Shenzhen University, Shenzhen, China. His current research interests include RF/microwave circuit and antenna design.

Dr. Wong was a recipient of the New Century Excellent Talents (NCET) in University Award, in 2013, and the Shenzhen Overseas High-Caliber Personnel Level C, in 2018. He serves as a Reviewer for several top-tier journals.

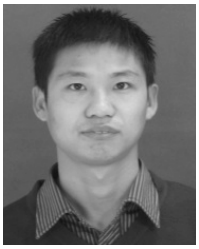

YIN LI (Member, IEEE) received the B.S. degree in applied physics from the China University of Petroleum, Dongying, China, in 2009, the M.Eng. degree in electromagnetic field and microwave technology from the University of Electronic Science and Technology of China (UESTC), Chengdu, China, in 2012, and the Ph.D. degree from the University of Macau, Macau, China.

From 2013 to 2015, he was a Research Assistant with The University of Hong Kong (HKU), Hong Kong. He is currently a Postdoctoral Research Fellow with the College of Electronics and Information Engineering, Shenzhen University, Shenzhen, China. His current research interests include numerical modeling methods of passive microwave circuits, computational electromagnetics, and microwave circuits, frequency selectivity surface, and filtering antenna.

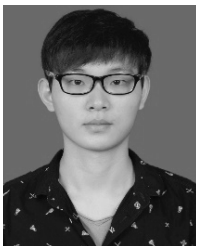

JING-YU LIN (Student Member, IEEE) received the B.E. degree from Southwest Jiaotong University (SWJTU), Chengdu, China, in 2016, and the M.E. degree from the School of Electronic and Information Engineering, South China University of Technology (SCUT), Guangzhou, China, in 2018. He is currently pursuing the Ph.D. degree with the University of Technology Sydney (UTS), Ultimo, NSW, Australia.

From October 2017 to February 2019, he was an Exchange Student with the University of Technology Sydney. His current research interest includes microwave cavity circuit design.

BAI-YANG LIU (Member, IEEE) was born in Dongguan, China, in 1990. He received the Ph.D. degree from the South China University of Technology, Guangzhou, China, in 2018.

He was a joint Ph.D. Student with the School of Electronic Engineering and Computer Science, Queen Mary University of London, London, U.K., in 2018. He was a Postdoctoral Research Fellow with the School of Electronic Engineering and Computer Science, Queen Mary University of London, in 2019. He is currently a Postdoctoral Research Fellow with the College of Electronics and Information Engineering, Shenzhen University, Shenzhen, China. His current research interests include orbital angular momentum multiplexing, rotational Doppler effect, spatiotemporally modulated meta-materials, and space-time-coding meta-surfaces.

FU-CHANG CHEN (Member, IEEE) was born in Fuzhou, China, in 1982. He received the Ph.D. degree from the South China University of Technology, Guangzhou, China, in 2010.

He is currently a Professor with the School of Electronic and Information Engineering, South China University of Technology. His current research interests include synthesis theory, design of microwave filters, and associated RF modules for microwave and millimeter-wave applications.

ZHI QUAN (Senior Member, IEEE) received the B.E. degree in communications engineering from the Beijing University of Posts and Telecommunications (BUPT), China, in 1999, and the Ph.D. degree (Hons.) in electrical engineering from the University of California, Los Angeles (UCLA), in 2009. He was a Visiting Scholar with the Department of Electrical Engineering, Princeton University, Princeton, NJ, USA, from 2007 to 2008. He was a Senior System Engineer with the Research and Development Department, Qualcomm Inc., San Diego, CA, USA, from 2008 to 2012. He was also a Senior RF System Engineer and Architect with Apple Inc., Cupertino, CA, USA, from 2012 to 2015. He is currently a Distinguished Professor with the College of Information Engineering, Shenzhen University. His current research interests include next-generation wireless communication systems, RF system calibration and measurement, the industrial IoT, edge computing, data-driven signal processing, and embedded machine learning. He was a recipient of the UCLA Outstanding Ph.D. Award, in 2009, the IEEE Signal Processing Society Best Paper Award, in 2012, and the China National Excellent Young Scientist Foundation, in 2016.